Field-frequency mapping of the electron spin resonance in the paramagnetic and antiferromagnetic states of $LaMnO_3$

László Mihály and Diyar Talbayev
Department of Physics and Astronomy, Stony Brook University, Stony Brook, New York 11794-3800, USA

László F. Kiss
Research Institute for Solid State Physics and Optics, POB 49, H-1525 Budapest, Hungary

Jianshi Zhou
Texas Materials Institute, University of Texas, Austin, Texas 78712-1063, USA

Titusz Fehér and András Jánossy
Budapest University of Technology and Economics Institute of Physics, and Solids in Magnetic Fields Research Group of the Hungarian Academy of Sciences, P.O. Box 91, H-1521 Budapest, Hungary

(Received 11 December 2002; revised manuscript received 3 October 2003; published 23 January 2004)

Electron-spin resonance has been studied in a stoichiometric single crystal of $LaMnO_3$ in the temperature range of 4.2 K–250 K. $LaMnO_3$ exhibits an extensively studied antiferromagnetic (AF) transition at $T_N = 141$ K. The spin resonance was detected both in a fixed-frequency microwave setup with various fixed frequencies (75 GHz, 150 GHz, and 225 GHz) in field-sweep mode or in a broad frequency band instrument at various fixed fields. The latter facility covers the far-infrared range with a lower cutoff frequency of 4 cm (120 GHz). Magnetic fields up to 14 T have been applied along the crystallographic *b* direction (the easy-axis direction in the AF state). The field dependence of the resonance is fully mapped and the results at low temperatures are well described by the AF resonance theory of Kittel and Keffer modified for the weak ferromagnetism. Deviations from the theory are evident at temperatures close to T_N. In the paramagnetic state the spin resonance is broad, and in addition to the expected paramagnetic signal around $g=2$, a temperature-dependent anomalous resonance has been also observed.

DOI: 10.1103/PhysRevB.69.024414 PACS number(s): 76.30.Fc, 75.50.Ee

I. INTRODUCTION

Stoichiometric and weakly doped $LaMnO_3$ are among the most extensively studied antiferromagnets.[1–9] Their orthorhombic *Pbnm* crystal structure can be derived from a simple cubic structure, where the three principal directions are parallel to the Mn-O-Mn bonds. In the orthorhombic phase the *c* direction corresponds to one of the original cubic directions whereas the orthorhombic *a* and *b* directions point along the face diagonals of the cubic reference cell. At 750 K a cooperative Jahn-Teller distortion results in a marked difference between the *a*, *b*, and *c* lattice parameters.[9,10] The magnetic moments located on the Mn ions order at the Néel temperature $T_N = 141$ K. In the first approximation, all moments within the *a*-*b* plane point in the same direction along (or opposite to) the *b* axis, which is the easy axis of magnetization. The antiferromagnetic order along the *c* direction doubles the *c* lattice parameter of the magnetic unit cell.[9]

In hole doped $LaMnO_3$ further symmetry breaking results in a canted antiferromagnetic (CAF) structure.[11–13] Instead of pointing exactly along the *b* axis, the moments slightly tilt in the *c* direction. Although the net moment is zero in the *b* direction (because of the alternating moments), and zero in the *a* direction (because all of the moments are perpendicular to *a*), there is a nonzero magnetization along the *c* axis. The canting gets smaller at lighter doping levels, and most experiments are consistent with very small or zero canting for the undoped stoichiometric compound.

There is a large body of literature on the electron-spin resonance (ESR) of pure and doped $LaMnO_3$.[13–20] Apparently, the ESR linewidth increases dramatically at low doping levels, and measurements on the pure material have been attempted in vain at 9 GHz, as the resonance line proved to be too broad.[16,17] High-field ESR was performed at 4.2 K in fields up to 25 T by Mitsudo *et al.*[18] and by Pimenov *et al.*[13,19,20]

In the present work, we first describe the main characteristics of our sample, the two instruments used in the spin-resonance studies, and we give a summary of the results in the form of complete maps of resonance absorption as a function of field and frequency at several temperatures. The methods used to evaluate the raw data are described next. A short introduction to the theory of antiferromagnetic resonance is given, and a comparison of the results in the low-temperature antiferromagnetic state to the theoretical predictions will follow. The high-temperature state will be discussed shortly. Finally we point out a few features that cannot be interpreted in terms of a simple antiferromagnetic or paramagnetic state.

II. $LaMnO_3$ SAMPLE

The single-crystal sample used in these studies has been grown at the University of Texas, Austin. The disk-shaped sample has been cleaved from a larger cylinder. The diameter of the disk is 4 mm, and the thickness is 0.6 mm. X-ray-

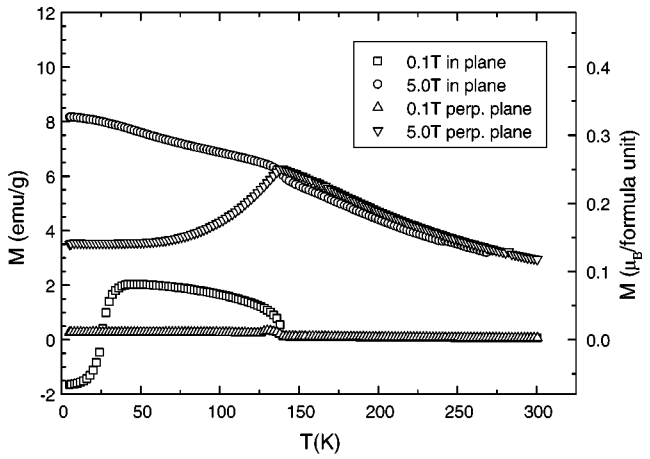

FIG. 1. Magnetization measurements in two fields (0.1 T and 5.0 T) and two orientations of the disk-shaped sample. If multiplied by a factor of 50, corresponding to the ratio of the two fields, the low-field magnetization coincides with the high-field data for $T > T_N$, as expected for a paramagnet with $M = \chi H$. For $T < T_N$ there is no such scaling. The weak ferromagnetic behavior is expected for field in the plane of the disk (see text). The magnetization should be proportional to the field for fields perpendicular to the disk. The observed deviation from strict proportionality can be attributed to a small twinned fraction of the sample, where the *c* axis is not in the plane of the disk.

diffraction measurements were used to determine the directions of the orthorhombic *a*, *b*, and *c* axes with respect to the sample disk. In particular, the *b* axis proved to be perpendicular to the disk.

The results of superconducting quantum interference device (SQUID) magnetization measurements are shown in Fig. 1. The magnetization was measured in two fields, 0.1 T and 5 T. First, the sample was oriented with the field perpendicular to the disk. At temperatures above the Néel temperature the magnetization scales with the external field, as expected. The low-temperature susceptibility is characteristic of an antiferromagnet with the magnetic field parallel to the easy axis, although in an ''ideal'' antiferromagnet the susceptibility (and magnetization) should approach zero at low temperature. Upon closer inspection one can see that below the Néel temperature the low-field and high-field magnetizations do not scale with the field. A likely explanation of this anomaly is that there is a small field-independent (ferromagnetic) term in the magnetization.

In the second measurement the external field was in the plane of the disk, although the orientation of the magnetic field relative to the crystallographic axes is unknown. We observe, again, that in the paramagnetic state the magnetization scales with the field, and the susceptibility is practically identical to the susceptibility measured with the field oriented in the *b* direction. The results in the paramagnetic state agree well with those of earlier studies.[17]

For an antiferromagnet with the easy axis perpendicular to the external field the susceptibility is typically a temperature-independent constant. Instead, at $T \ll T_N$ the low-field measurements show evidence for a strong and temperature-dependent ''ferromagnetic'' magnetization. This component dominates the low-field measurement, causing a large negative (i.e., opposite to the external field) magnetization at the lowest temperatures which is reversed at about 20 K. Since in this particular measurement the sample was initially cooled in zero field, and warmed in a field during the measurement, the negative contribution may very well be the result of a residual spontaneous magnetization. This observation is consistent with the CAF magnetic structure, if the (pseudo-ferromagnetic) *c* axis is not exactly perpendicular to the external field. At 5 T field the negative component is not present, but the enhanced magnetization (relative to the temperature-independent value expected for an AF) is likely the result of a similar ferromagnetic component. In a single-crystal study Skumryev *et al.* measured a ferromagnetic magnetization of 0.18 μ_B/f.u. at 5 T field along the *c* axis[21] (f.u. stands for formula unit, and each formula unit contains one Mn ion). The maximum value seen in Fig. 1 corresponds to a smaller value 0.08 μ_B/f.u. The difference is due to the fact that we did not orient the magnetic field exactly parallel to *c*.

At 5 T the difference of the magnetizations belonging to the two field orientations is 0.18 μ_B/f.u. We interpret this in terms of the difference between the easy-axis and perpendicular susceptibilities. Indeed, Skumryev *et al.* measured a similar value 0.22 μ_B for the difference between the magnetizations along the *a* and *b* axes.

The magnetization results are therefore consistent with the assumption that the vast majority of the sample is oriented with the orthorhombic *b* axis perpendicular to the surface of the disk. The presence of a small but significant ferromagnetic component in this direction suggests that the sample is slightly twinned so that in a small volume fraction the *c* axis is not parallel to the plane of the disk. A plausible twinning mechanism leads to a matching of the orthorhombic $\langle 001 \rangle$ and $\langle 110 \rangle$ directions, as reported in other single crystals, including the one used in the neutron studies of Moussa *et al.*[9] In this case the *c* axis of the minority twin phase makes a 45° angle with the surface.

An alternative explanation of the observed magnetization curves may be that the sample is single phase, but the orientation of the *b* axis is not exactly perpendicular to the disk surface. As we will show later, this assumption proves to be inconsistent with the low-temperature antiferromagnetic resonance (AFMR) observations.

III. INSTRUMENTS

The electron-spin resonance has been detected by measuring the attenuation of electromagnetic radiation transmitted through a disk-shaped sample. Two types of instruments have been used in this study. In the first one, the absorption was measured as the function of magnetic field (for fields up to 9 T) at three frequencies (75 GHz, 150 GHz, and 225 GHz). The setup is illustrated in Fig. 2. The main components of this device are the quartz stabilized microwave source (Gunn diode) and a 9 T Oxford Instruments superconducting magnet. The microwave power is chopped with a p-i-n diode at audio frequencies (typically 20 kHz), and the transmitted signal is detected by a QMC Inc. InSb hot elec-

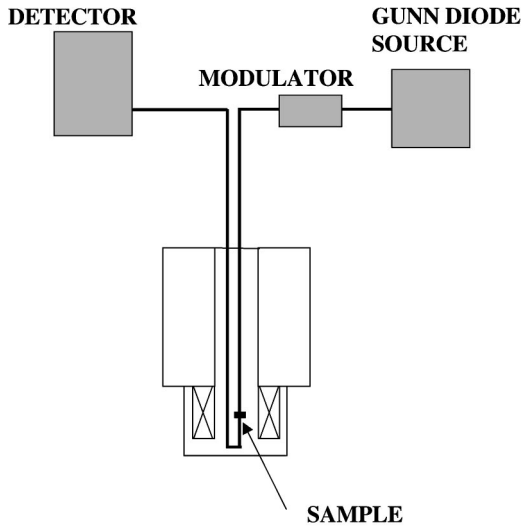

FIG. 2. Schematic representation of the high-field ESR instrument used in this study. The instrument, located at the Budapest University of Technology and Economics, was used at fixed frequencies (75 GHz, 150 GHz, and 225 GHz) with fields up to 9 T.

tron detector, followed by a lock-in amplifier.

The second instrument combines a very bright broadband light source with a far-infrared spectrometer and a superconducting magnet (see Fig. 3). The instrument has been installed at the National Synchrotron Light Source in Brookhaven National Laboratory.[22] The light from the synchrotron is guided by planar and focusing mirrors to the Sciencetech SPS200 Fourier transform IR (FT-IR) spectrometer. The large (10 cm) mirror size of this device limits the diffraction effects and is particularly important for long-wavelength operation. The light from the spectrometer is focused into a 14-mm-diameter cylindrical light pipe that guides the radiation to the vertical-bore Oxford Instruments Spectromag 16 T superconducting magnet. The light pipe and the spectrometer are placed under rough vacuum. The radiation passes two wedged single-crystal quartz windows and enters the variable temperature insert (VTI), and it is guided vertically upwards from the bottom of the magnet by light pipe segments. The sample is sandwiched between two light cones inside the VTI, at the center of the magnet. The light cones match the light pipe to the 4-mm-diameter circular aperture that is completely covered by the sample. The radiation is detected by a He cooled doped silicon bolometer (made by IR Laboratories), placed at the upper end of the light pipe, at the top of the magnet. The detector has a cold filter (black polyethylene) and operates at 1.2 K with a He reservoir separate from the magnet.

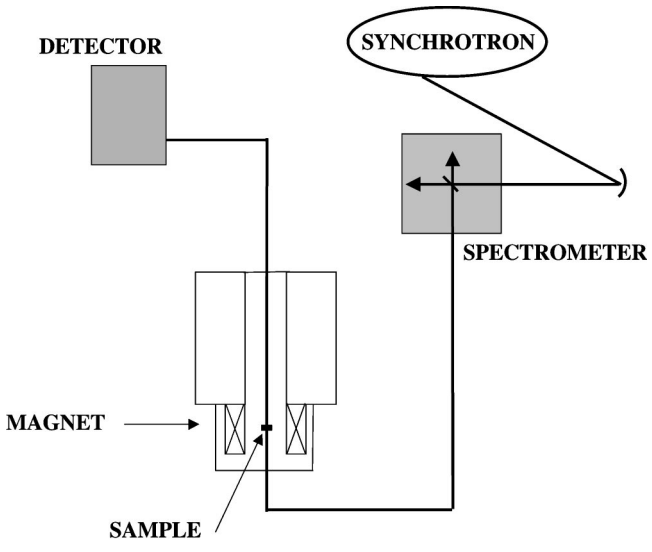

FIG. 3. Schematic representation of the magneto-optical far-infrared spectroscopy instrument used in this study. The instrument, installed at the National Synchrotron Light Source of the Brookhaven National Laboratory, covers frequencies ranging from 1 cm^{-1} (30 GHz) with fields up to 16 T.

We use a room-temperature fluorogold filter of appropriate thickness to set the high-frequency cutoff between 30 cm^{-1} and 40 cm^{-1}. The relatively small sample size in the present study resulted in a lower cutoff frequency of 4 cm^{-1}. [In test measurements with large samples the lowest frequency with measurable signal level was 2 cm^{-1} or 60 GHz (Ref. 22).] In FT-IR spectroscopy the frequency resolution of the spectrum is variable, as it is determined by the path length of the moving mirror. Since the spin-resonance linewidth in this sample is about 1 cm^{-1}, we selected 0.5-cm^{-1} (apodized) resolution in these studies.

The direction of the static magnetic field is parallel to the direction of the propagating microwave/IR radiation. In this geometry, although the polarization of the electromagnetic radiation is not fully controlled, the exciting rf magnetic field is approximately perpendicular to the static field. A more complex electromagnetic field pattern may develop at the edge of the sample, in the vicinity of the light cones directing the light into the sample. These edge effects become significant at long wavelengths, when the sample size is comparable to the wavelength.

The antiferromagnetic resonance can be studied in zero external field by the traditional methods of far-infrared spectroscopy, as introduced by Richards, Tinkham, and others.[23,24] We also performed a few measurements without magnetic field in a simple transmission setup, outside the magnet. The sample was placed on a 4-mm-diameter aperture and attached to the cold finger of a Helitran continuous flow cryostat, between the two polyethylene windows of the cryostat. The light from the spectrometer was directly focused onto the sample. The detector (a 1.2-K bolometer) was placed in close proximity of the sample, right next to the output window.

IV. EVALUATION OF FT-IR SPECTRA

Background corrections, i.e., corrections of the spectra for intensity variations of the light incident onto the sample and caused by multiple reflections within the sample, are of primary importance in quantitative IR spectroscopy. In the transmission geometry, the most common method involves dividing two ''raw'' power spectra: one in the presence of the sample and the other measured with an empty aperture. For

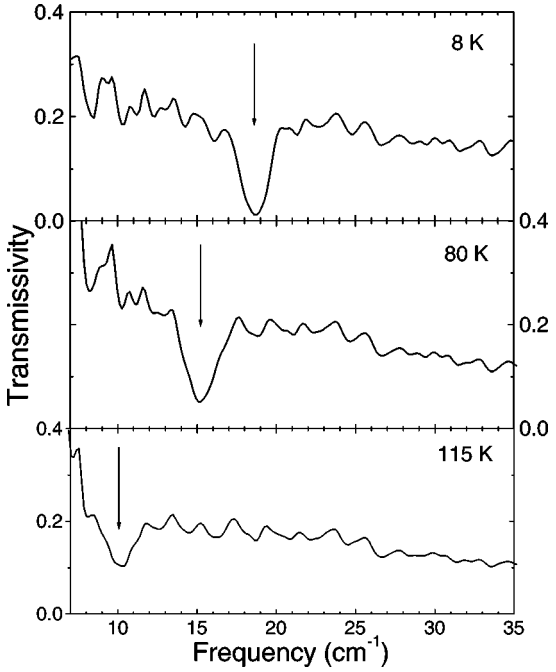

FIG. 4. The transmissivity of the sample in zero magnetic field at several temperatures. The strong, temperature-dependent dip, marked by the arrow, is due to the antiferromagnetic resonance.

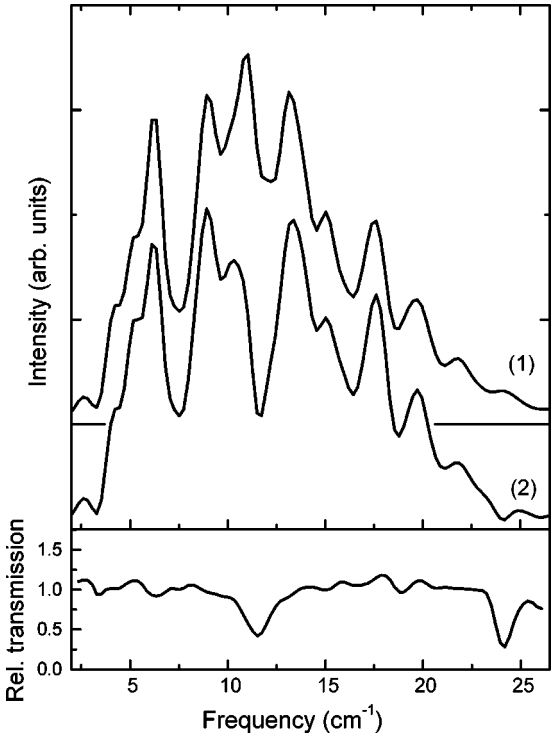

FIG. 5. Raw power spectra detected with a 30-cm^{-1} upper cutoff filter at the detector. Most of the features seen in these curves are due to the combination of the synchrotron power spectrum, detector sensitivity, and other instrumental effects. Curve (1) corresponds to $T=180$ K, and $H=0$ T; curve (2) was recorded at $T=50$ K, $H=7$ T. The magnetic absorption lines appear as extra ''dips'' in the second curve. The lower panel shows the relative transmission, i.e., the ratio of the curves (2) and (1).

spectra taken in zero magnetic field outside the magnet we used this method. The transmissivity obtained this way is shown in Fig. 4 at a few representative temperatures. The strongly temperature-dependent absorption line is due to the AF resonance and will be discussed later in detail. The wavy pattern on each spectrum is due to the interference between light beams reflected from the surfaces of the sample. Since these surfaces are not perfectly planar, the interference pattern is irregular, although it is quite reproducible. The overall transmission is about 20% and decreases at higher frequencies. (The sample becomes opaque above 100 cm^{-1} due to multiphonon absorption processes.)

In the spin-resonance studies we found two ways for taking care of the background corrections. To illustrate the first way, in Fig. 5 we show two raw spectra of $LaMnO_3$ taken with light pipes guiding the radiation through the magnet. The upper curve represents the transmitted intensity at $T=180$ K in zero magnetic field, and the lower curve represents the same quantity at 50 K in 7 T field. Most of the structure seen in these spectra is due to instrumental effects, including the spectrum of the synchrotron radiation, the interference patterns developing in the light path, the filtering, and the detector sensitivity. We can distinguish in the $T=50$ K, $H=7$ T spectrum (Fig. 5) two AFMR absorption lines (one line at 12 cm^{-1} and the other at 24 cm^{-1}), when we compare it to the $T=180$ K and $H=0$ spectrum, there is no magnetic resonance at any frequency. The figure also shows that the overall absorption of the sample, apart from magnetic-resonance effects, is independent of temperature. Since high-temperature ($T>T_N$) low-field ($H\leqslant 3$ T) spectra have no signs of magnetic-resonance absorption, we can use these spectra as a background. In order to further average out the noise in the spectra, we define our background to be the average of eight spectra: four spectra taken at 160 K with 0, 1, 2, 3 T magnetic fields and four spectra taken at 180 K at the same fields. We divide all our data by the background defined this way and use the term ''relative transmission'' (I_r) to denote the ratio (as opposed to transmissivity shown in Fig. 4).

At the lowest temperatures and highest fields (14 T) the eigenfrequency of the upper branch of the AFMR line increases beyond the 30-cm^{-1} cutoff set for the higher-temperature measurements. Therefore, the upper cutoff in the 15-K measurements was increased to about 40 cm^{-1}. The background defined earlier is of no use in this case, so we used a different procedure to process the 15-K spectra. To construct a suitable background, we notice that the AFMR frequency is strongly field dependent. Since the signal is confined to rather narrow regions of the spectra (~ 2 cm^{-1}), one could use the AFMR spectra at high fields as a background in the analysis of the spectra at zero or low fields and vice versa. Alternatively, in an approximate but very convenient way, if spectra are measured at many different fields, one can choose the background to be the average of all the spectra. Thus, we define our background at 15 K to be the average of all spectra taken at 15 K (Fig. 6). After dividing the 15-K spectra by this background, we obtain the relative transmission defined earlier (Fig. 6, lower panel).

The relative transmission data can be directly related to

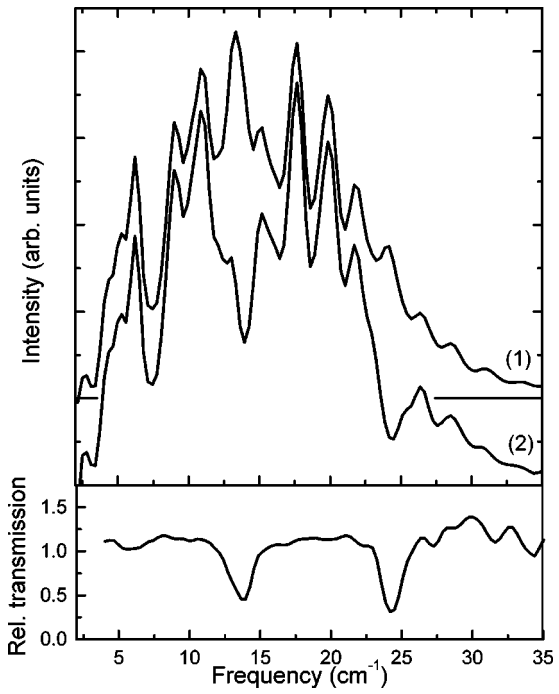

FIG. 6. Transmission spectra taken at $T=15$ K with 40-cm^{-1} upper cutoff. Curve (1) is the background defined as the average of all spectra taken at different magnetic fields at $T=15$ K. Curve (2) is the $T=15$ K spectrum with $H=6$ T. The lower panel shows the relative transmission—the ratio of the curves (2) and (1).

the spin resonance. We start with the dimensionless magnetic susceptibility in the form discussed by Slichter,[25]

$$\chi' = \mathrm{Re}\,\chi = \frac{\chi_0 \omega_0 T_2}{2} \frac{(\omega_0-\omega)T_2}{1+(\omega-\omega_0)^2 T_2^2}, \tag{1}$$

$$\chi'' = \mathrm{Im}\,\chi = \frac{\chi_0 \omega_0 T_2}{2} \frac{1}{1+(\omega-\omega_0)^2 T_2^2}, \tag{2}$$

where ω_0 stands for the resonance frequency, T_2 is the relaxation time that defines the width of the absorption line, and χ_0 is the static magnetic susceptibility in the direction of the rf field (in our case, perpendicular to the easy magnetization direction). The decay of the electromagnetic wave propagating in the bulk material can be described using the notion of complex index of refraction, defined as $\hat{n}=\sqrt{\varepsilon\mu}$, where ε is the dielectric function and $\mu=1+4\pi\chi$ is the magnetic permeability. The order of magnitude of χ at the resonance frequency can be estimated from Eq. (1):

$$\chi \sim \frac{\chi_0 \omega_0 T_2}{2} \simeq 0.01, \tag{3}$$

where we used 2 cm^{-1} and 12 cm^{-1} as the values of the resonance linewidth and frequency respectively, and the static susceptibility $\chi_0=0.0008$ was determined directly from the SQUID measurements discussed earlier. Since $4\pi\chi \ll 1$, one can expand $\hat{n}$ as

$$\hat{n}=\sqrt{\varepsilon\mu}=\sqrt{\varepsilon}(1+2\pi\chi)=\sqrt{\varepsilon}+2\pi[\mathrm{Re}(\sqrt{\varepsilon})\chi'-\mathrm{Im}(\sqrt{\varepsilon})\chi''] + i2\pi[\mathrm{Re}(\sqrt{\varepsilon})\chi''+\mathrm{Im}(\sqrt{\varepsilon})\chi'].$$

As the thickness of the sample is known, we can estimate the value of the (real) index of refraction, $n=\mathrm{Re}(\sqrt{\varepsilon})$, from the distance between the multiple reflection interference peaks in the absolute transmission spectra (Fig. 4) and we find $n\approx 4$. Similarly, Ivanov[26] finds the dielectric constant of $LaMnO_3$ to be $\varepsilon\approx 20.5$ at $T=80$ K and frequency of 14 cm^{-1}, which corresponds to $n\approx 4.5$. These estimates allow us to identify the leading terms in the real and imaginary parts of refractive index $\hat{n}$ to be

$$\hat{n}=\sqrt{\varepsilon}+i2\pi\mathrm{Re}(\sqrt{\varepsilon})\chi''.$$

Under our experimental conditions the transmittance of the sample in terms of the complex index of refraction is

$$T \approx \left(1-\left|\frac{n-1}{n+1}\right|^2\right)^2 \exp[-2(\mathrm{Im}\,\hat{n})d\omega/c], \tag{4}$$

where the factor $(1-|n-1/n+1|^2)^2$ represents the decrease in intensity due to the reflection of the light, and the exponential term describes the absorption inside the sample of thickness d. The approximate nature of this expression is obvious from the fact that it does not reproduce the interference pattern discussed before. To justify the use of Eq. (4) we performed computer simulations with the exact transmission formula. The approximate formula proved to be satisfactory in our parameter range. This is often the case when there is significant damping of the radiation within the sample.

In the absence of the magnetic resonance $\chi=0$ and $\hat{n}=\sqrt{\varepsilon}$. Therefore, by dividing the resonance spectra by the background spectra we obtain a quantity proportional to $\exp[-4\pi\mathrm{Re}(\sqrt{\varepsilon})d\chi''\omega/c]$ with d being the thickness of the sample. Taking the negative logarithm of the relative transmission I_r we obtain

$$-\ln(I_r)=\frac{4\pi n d\chi''\omega}{c}, \tag{5}$$

where $n=4$ is the real part of the refraction index. We can use the imaginary part of the magnetic susceptibility in the form (2) to carry out a least-squares fitting procedure to find the values of the resonance frequencies ω_0 and the parameters χ_0 and T_2. As an example, Fig. 7 shows the fit and the parameter values obtained this way for the spectrum at $T=50$ K and magnetic field $H=7$ T. As discussed earlier, χ_0 is the static susceptibility in the direction perpendicular to the easy axis. The result of the fit is $\chi_0=0.000\,47$ (Fig. 7).

This value can be compared to the static susceptibility measurements of Fig. 1. We estimate the value of the static dimensionless susceptibility (cgs units) at T_N using the measured mass of our sample (42 mg) and the mass density of $LaMnO_3$ of 6.64 g/cm^3. The density has been calculated with the values of the magnetic unit-cell parameters $a=0.553$ nm, $b=0.575$ nm, $c=0.766$ nm, taken from the

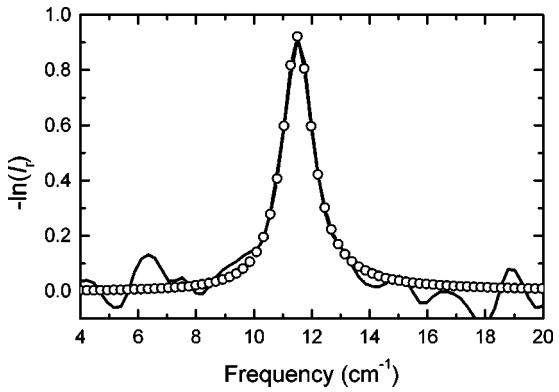

FIG. 7. The solid curve is the absorption coefficient evaluated from the measured relative transmission (at $T=50$ K and $H=7$ T) as $-\ln(I_r)$. The open circles represent a least-squares fit with χ'' given in Eq. (2). The fit yields $\omega_0=11.48\ \mathrm{cm}^{-1}$, $\chi_0=0.00047$, and $T_2=1.57$ cm.

neutron-scattering study of Moussa.[9] At the AF transition temperature the susceptibilities along and perpendicular to the easy axis are the same, and we find the value to be 0.0008. The agreement is reasonable.

A representative set of the IR transmission results is shown in Fig. 8. The darker color on these maps of the magnetic field-frequency plane indicates stronger magnetic absorption. To assemble the maps, at each temperature 15 frequency scans were recorded at fixed fields between 0 T and 14 T, in 1-T steps. A typical scan at a fixed magnetic field lasted about 1.5 min; a full set of 15 scans at a fixed temperature, including the sweep time of the magnet, took about 45 min.

In the paramagnetic state the resonance follows the expected $\hbar\omega=g\mu_B H$ linear dependence on the magnetic field, with $g=2$. The full width at half maximum of the resonance is of the order of 1.5 T. The finite frequency modes corresponding to the two coupled sublattices are visible in the AF state. To our knowledge this is the first mapping of the AF resonance in such a great detail. These results, supplemented with more experimental data, will be discussed in the following sections.

V. SPIN RESONANCE IN THE ANTIFERROMAGNETIC STATE

The theory of AFMR was established in the 1950s by a number of authors.[27,28] In the absence of an external field, the resonance frequency of an antiferromagnet with uniaxial anisotropy is given by

$$\omega_0=\gamma\sqrt{H_a(H_a+2H_e)}, \tag{6}$$

where $\gamma=g\mu_B/\hbar$, and H_a and H_e are the phenomenological anisotropy and exchange fields, respectively. For the case

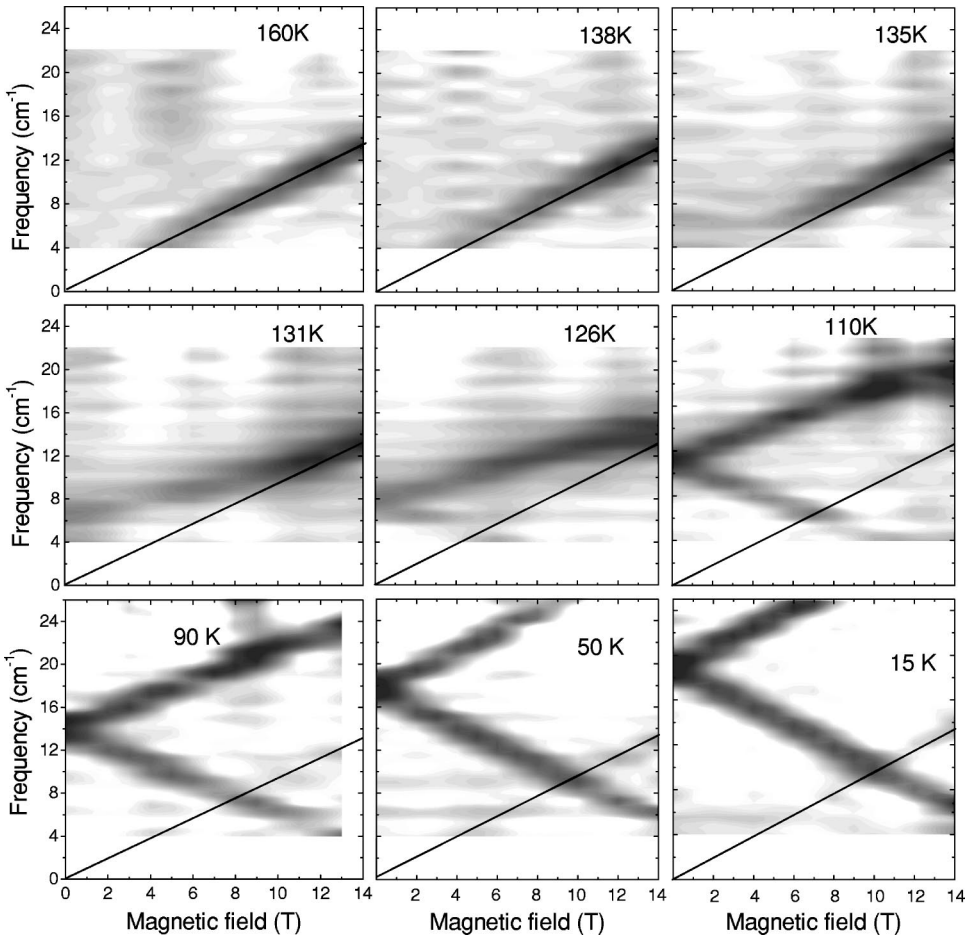

FIG. 8. Power absorption due to magnetic resonance as a function of field and frequency at several representative temperatures. The frequency resolution was 0.5 cm^{-1}, the magnetic field was varied in 1-T steps. Darker shades indicate stronger absorption.

most relevant to the present study, when the external field is applied along the easy axis of the magnetization, the AFMR frequency is

$$\omega^{\pm} = \gamma \sqrt{H_1^2 + \frac{(\alpha H)^2}{2}} \pm \gamma H \left(1 - \frac{\alpha}{2}\right), \tag{7}$$

where $H_1 = \sqrt{H_a(H_a + 2H_e)}$ (or $H_1 = \sqrt{2H_a H_e}$ if $H_a \ll H_e$) and $\alpha = \chi_\parallel / \chi_\perp$ ($\chi_\parallel$ and $\chi_\perp$ are the susceptibilities parallel and perpendicular to the easy axis). The two branches of the resonance spectrum (represented by the "$-$" and "$+$" signs in the equation) are due to a nontrivial combination of the external, anisotropy, and (time-dependent) exchange fields, acting on the two sublattice magnetizations parallel and opposite to the external field.[27] The normal modes of the sublattice motion that correspond to the $+$ sign in Eq. (7) represent the clockwise circular precession of the magnetization of both sublattices about the direction of the magnetic field. Similarly, the normal modes corresponding to the $-$ sign represent the circular precession of the sublattice magnetizations in the counterclockwise direction. This structure of the normal modes suggests that the upper or lower branch of the spectrum can be excited selectively by light circularly polarized in one or the opposite direction. In our measurements we used unpolarized light and, therefore, observed both branches of the resonance spectrum.

Equation (7) holds until the field H reaches the value of the critical spin-flop field $H_{sf} = \sqrt{2H_a H_e/(1-\alpha)}$. At fields just below the spin-flop transition the lower branch of the resonance reaches zero frequency. At $H = H_{sf}$ the spin system becomes unstable in its original orientation along the easy axis. At higher fields the spins align perpendicular to the external field, and the two modes are degenerate:

$$\omega^{\pm} = \gamma \sqrt{H^2 - H_{sf}^2}. \tag{8}$$

The zero-field AFMR frequency corresponds to spin-wave frequency at zero wave number. In order to interpret the observed spin-wave spectra, Moussa[9] solved the model Hamiltonian

$$H = -\sum_{i,j} J_{ij}(S_i S_j) - D\sum_i S_i^{z2} \tag{9}$$

in the low-temperature limit, using the Holstein-Primakoff approximation. Only two types of nearest-neighbor exchange couplings were considered: the ferromagnetic in-plane coupling, J_1, and the antiferromagnetic coupling along the c direction, J_2. The last term in Eq. (9) represents the uniaxial single-ion anisotropy. For zero wave number one obtains

$$\hbar\omega_0 = 2S\sqrt{D(D - 4J_2)}. \tag{10}$$

The anisotropy and exchange fields introduced earlier are related to these coupling constants as $H_a = 2SD/\hbar\gamma$ and $H_e = -4SJ_2/\hbar\gamma$. Note that the factors 2 and 4 correspond to the number of nearest neighbors along the c axis and in the a-b plane, and for antiferromagnetic coupling J_2 is negative. Another interesting point is that the anisotropy is entirely determined by the single-ion term, and the exchange anisotropy is assumed to be zero in this model.

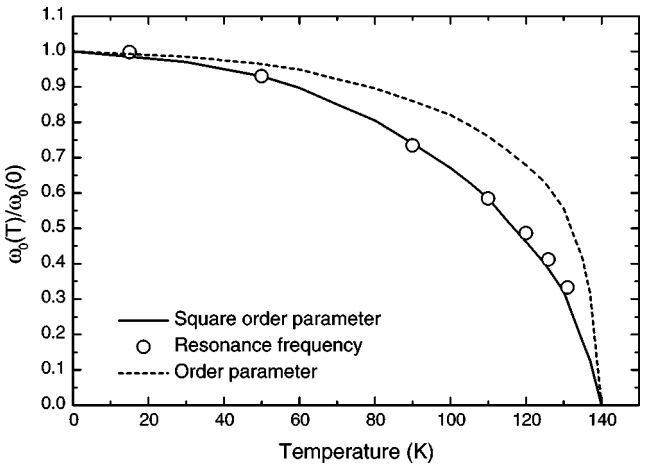

FIG. 9. Temperature dependence of the zero-field antiferromagnetic resonance frequency. This frequency is compared to the order parameter of the AF transition, defined as the square root of the diffraction intensity of the superlattice diffraction peak in the neutron-scattering measurements of Moussa *et al.* (Ref. 9). (The diffraction intensity at low temperature was scaled to the low-temperature value of the resonance frequency.) Clearly, the AF resonance frequency scales with the diffraction intensity itself, i.e., the square of the order parameter.

The Dzyaloshinsky-Moriya[29,30] coupling may cause a canting of the sublattice magnetization in the c direction and influences the spin-resonance frequencies.[31] This effect is further enhanced by de Gennes's double-exchange[32] interaction. In the CAF structure the symmetry breaking splits the zero-field resonance frequency.[13,18,19,31] The canting is strong enough in hole doped $LaMnO_3$ to cause a visible splitting of this kind.[13] However, the zero-field splitting in the undoped sample is very small, smaller than the linewidth of the resonance. We will neglect the effects of the CAF structure when we evaluate the results with the static magnetic field along the easy axis.[9,18]

First we will discuss the zero-field antiferromagnetic resonance, appearing as prominent absorption lines in the absolute transmission data shown in Fig. 4, and corresponding to the $H = 0$ cuts on the maps of Fig. 8. In the frequency range available to us, the AF resonance was observed at temperatures ranging from 8 to 131 K. There is no significant temperature dependence below 30 K, and in the low-temperature limit the AF resonance frequency is

$$\omega_0/(2\pi c) = 18.2 \pm 0.2 \ \ \mathrm{cm}^{-1}. \tag{11}$$

This value agrees with the $q = 0$ frequency of spin waves measured by Moussa[9] ($\sim$0.6 THz). The exchange and anisotropy fields measured in the ESR study of $LaMnO_3$ by Mitsudo[18] yield the zero-field resonance frequency of 18.3 cm^{-1}, and the frequency measured by Ivanov, Mukhin *et al.*[19,26] is also about 18 cm^{-1}.

The frequency of the zero-field resonance as a function of temperature is shown in Fig. 9. There is an apparent agreement between the temperature dependence of the mea-

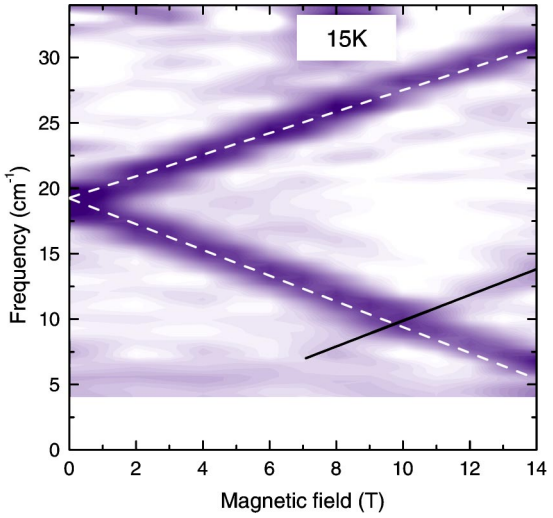

FIG. 10. Field dependence of the antiferromagnetic resonance frequency at low temperatures. The dashed lines represent Kittel's theory (Ref. 27). The solid line indicates resonance at $g=2$.

sured frequency and that of the intensity of the magnetic superlattice Bragg scattering, determined in neutron-scattering studies.[9] In the framework of the simple models discussed above, this agreement is unexpected, since the neutron-scattering intensity is proportional to the square of the sublattice magnetization M_1, whereas no such simple relationship exists for the AF resonance frequency.

The field dependence of the resonance is compared to the theoretical predictions [Eq. (7)] at two temperatures in Figs. 10 and 11. At low temperature the results are similar to those of Mitsudo,[18] and the agreement with theory is near perfect.

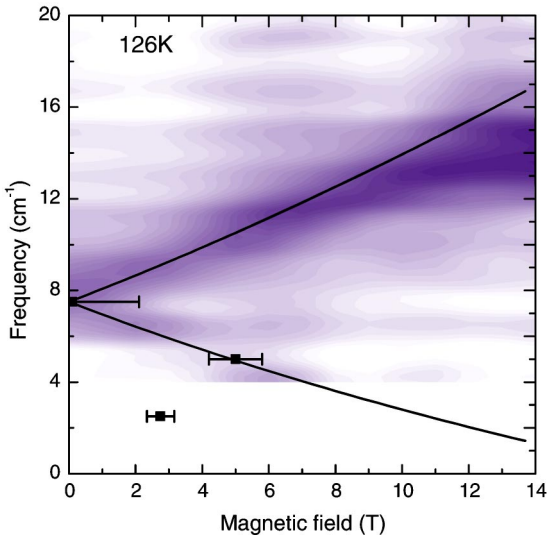

FIG. 11. Summary of far-IR and fixed-frequency high-field ESR measurements at 126 K. The strong resonances seen at 225 GHz (7.5 cm^{-1}) and 150 GHz (5.0 cm^{-1}) are indicated by the horizontal bars. Similar good agreement between the FT-IR and fixed-frequency measurements was found at other temperatures. At higher magnetic fields there is an observable difference between the experiment and the theory (solid line).

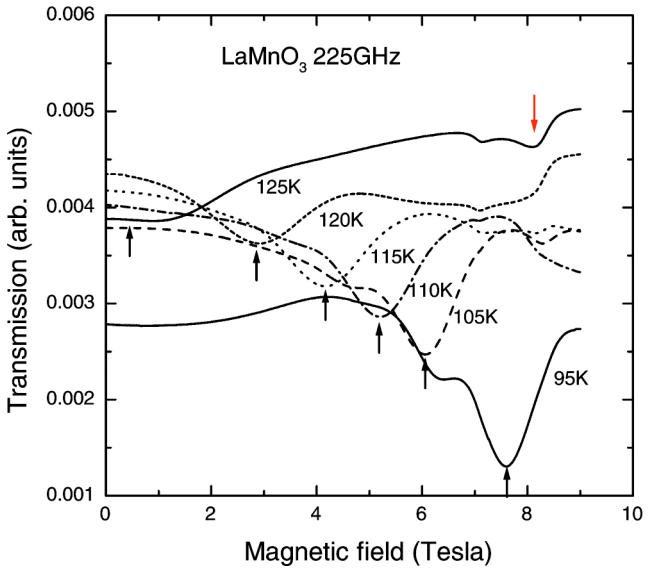

FIG. 12. ESR signal as a function of magnetic field at 225 GHz for several temperatures as indicated in the figure. The $g=2$ paramagnetic resonance appears at 8.1 T. A signal is seen, especially at lower temperatures, around this value. The antiferromagnetic resonance results in a strong, temperature-dependent absorption, with a resonance field increasing from ≈ 0 T at 125 K to about 7.6 T at 95 K. In the low-temperature data there is a secondary, weaker resonance at slightly lower fields. The weak and relatively sharp dip seen at 125 K slightly above 7 T is due to an instrumental effect.

As the temperature is raised, the zero-field resonance frequency decreases with increasing temperature. Initially the field dependence still corresponds to the theory, see Fig. 8. However, important deviations from the calculations become apparent close to the transition temperature. At 126 K the measured resonance absorption does not increase in frequency as much as expected (Fig. 11), and the discrepancy is even more prominent at 135 K (Fig. 8). At $T=138$ K the sample is certainly below the Néel temperature, but in the measured range of frequencies (Fig. 8) the spin-resonance signal cannot be distinguished from the paramagnetic resonance.

The disagreement of the experiment and the simple theory is understandable, since the theory assumes that the exchange field is much larger than the external field. This is a good approximation at low temperatures, when the exchange field is in the 40-T range. However, at temperatures close to T_N the exchange field must approach zero, and the theory fails, as H_e becomes comparable to the applied field (14 T).

The results obtained by the IR transmission method (Fig. 8) can be combined with the high-field ESR studies at fixed frequencies. A representative set of field-sweep measurements at 225 GHz is shown in Fig. 12. The antiferromagnetic resonance results in a strong, temperature-dependent absorption, with a resonance field increasing from 0 T at 125 K to about 7.6 T at 95 K. In the low-temperature data there is a secondary, weaker resonance at slightly lower fields. A similar behavior has been observed at 150 GHz. At both frequencies there is a clearly visible and strongly temperature-dependent resonance that appears at zero field at a

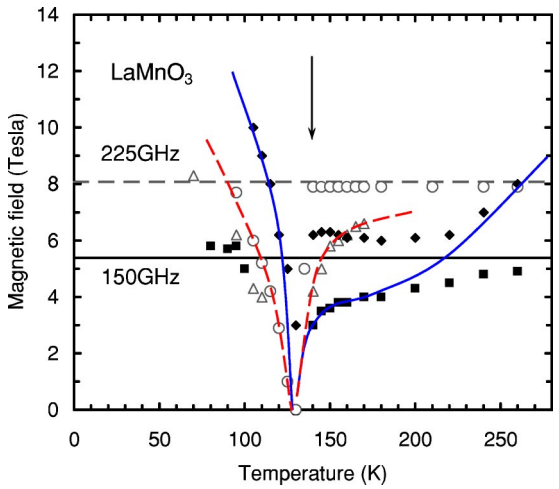

FIG. 13. Summary of the ESR data obtained by magnetic-field sweeps at 150 GHz and 225 GHz. Open symbols and dashed lines belong to 225 GHz; full symbols and solid lines belong to 150 GHz. The horizontal lines indicate the resonance field corresponding to $g=2$. The vertical arrow marks the Néel temperature. The behavior characteristic of two intersecting modes is visible in the 225-GHz data in the 200 K–240 K region.

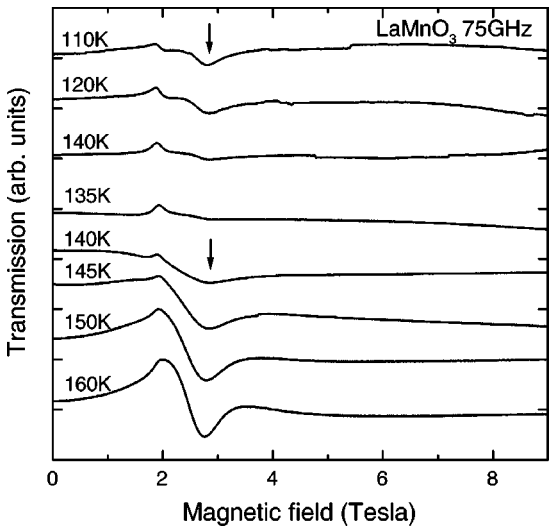

FIG. 14. Magnetic resonance at 75 GHz. At this low frequency no AF resonance is observed. The paramagnetic resonance, indicated by an arrow at the 160-K curve, broadens beyond recognition just below the Néel temperature (see the 135-K data). A peak resembling a paramagnetic resonance appears well below T_N. The peak around 1.9 T is due to an instrumental effect.

temperature slightly below T_N, with the resonance field rapidly increasing at lower temperatures. The 75-GHz scans also exhibited anomalies at temperatures below T_N, but the features were too broad, and the temperature variations were too fast to follow. Figure 13 provides a summary of the results obtained by magnetic-field sweeps at 225 GHz and 150 GHz. (The behavior above T_N will be discussed later.)

Figure 11 illustrates that the results obtained by the two different methods (high-field ESR sweeps and far IR-field-frequency mapping) are perfectly consistent. At 126 K the 225-GHz and 150-GHz absorptions lie on the lower branch of the AF resonance curve. For $T<T_N$, the strong temperature dependence of the resonance field in Fig. 13 is well understood in terms of the temperature dependence of the zero-field resonance frequency ω_0 and the overall field-frequency map in Fig. 8: as ω_0 increases with lowering temperature, the crossing of the lower branch of the resonance and the constant frequency line moves to higher and higher fields.

VI. PARAMAGNETIC STATE

The high-temperature field-frequency maps of Fig. 8 illustrate the expected linear relationship between field and frequency corresponding to approximately $g=2$. The fixed-frequency data (Figs. 14–16) show, in addition to the $g\approx 2$ line, some weaker anomalous features, discussed in the following section. The linewidth is about 1 T, similar to the linewidth in the AF state, and in agreement with the work of Mitsudo *et al.*[18] but larger than that found by Huber *et al.*[33]

A thorough discussion of the role of the various interactions leading to the strong line broadening in the paramagnetic state is given in Ref. 33. Roughly speaking, the anisotropy term in Eq. (9) causes line splitting or broadening in the paramagnetic state of the undoped insulator with negligible exchange between ions. The paramagnetic resonance absorption of an isolated Mn^{3+} $S=2$ spin ion is expected to split into four lines at distances $\pm D$ and $\pm 3D$ in a crystal field of tetragonal symmetry with $H||c$ [here D is the anisotropy parameter in Eq. (9)]. In $LaMnO_3$ $D=1.3$ T (Ref. 9) has been determined from inelastic neutron-scattering data. The corresponding splitting should be seen in the experiment, since it is larger than the observed linewidth. Therefore, we conclude that in the paramagnetic state there is enough interaction between the Mn ions and/or enough residual mobile holes to

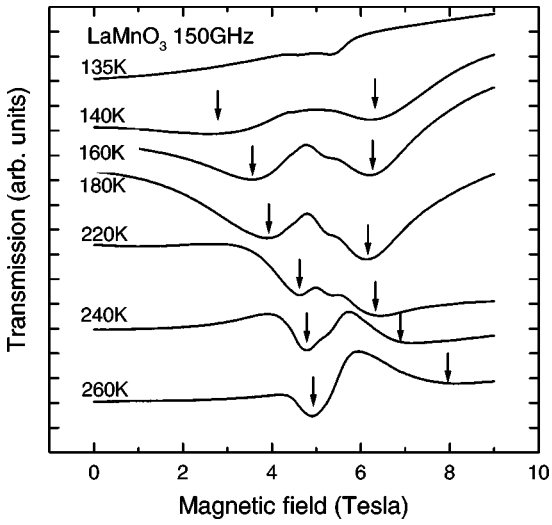

FIG. 15. Magnetic resonance at temperatures above the Néel temperature at 150 GHz. There are two resonance lines, indicated by the arrows. In contrast to the 225-GHz data, both lines exhibit temperature dependence. The positions of the arrows follow a behavior characteristic of ''level crossing.''

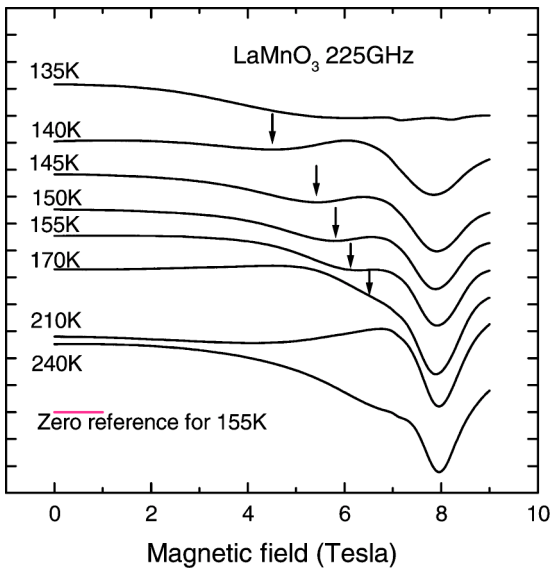

FIG. 16. Magnetic resonance at temperatures above the Néel temperature at 225 GHz. Two resonance lines are apparent. One of them remains at constant field, around the value corresponding to $g=2$. The other one (indicated by arrows) exhibits a strong temperature dependence.

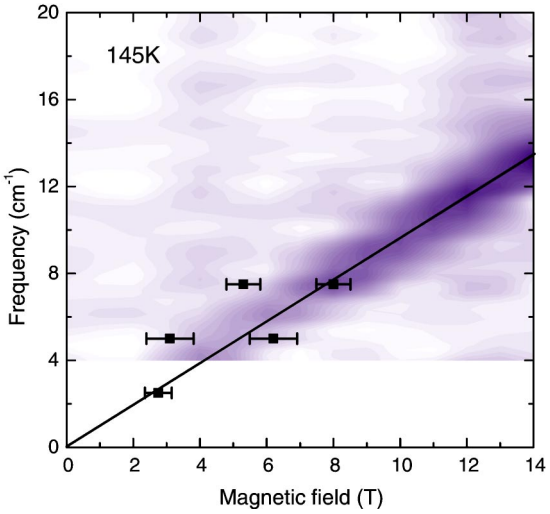

FIG. 17. Comparison of the far-IR and fixed-frequency data above the Néel temperature. The IR absorption measurement shows a broad line, following $g=2$. The fixed-frequency measurements at 225 GHz (Fig. 16) and 150 GHz (Fig. 15) exhibit two peaks. The 75-GHz data (Fig. 14) fall on the $g=2$ line.

cause a significant motional narrowing of the fine structure, resulting in a single resonance line.

VII. ANOMALOUS MAGNETIC-RESONANCE MODES

The major part of our paper describes the method of mapping magnetic-resonance modes into two-dimensional magnetic field-frequency diagrams using a synchrotron source and far-infrared spectroscopy and a comparison with fixed-frequency ESR spectroscopy. Although there were magnetic-resonance studies in the past, there was no comprehensive work on the temperature and magnetic-field dependence in both the antiferromagnetic and paramagnetic phases of a high quality $LaMnO_3$ single crystal. Our results are in general confirming the findings of the previous studies. However, some rather puzzling effects are also found. In addition to the expected antiferromagnetic and paramagnetic modes, some resonance modes that cannot be ascribed to the bulk of an ideal $LaMnO_3$ crystal are also found. These have an anomalous temperature dependence with rather unusual characteristics below and above the Néel temperature. Some of these anomalous resonances are not resolved in the FT-IR spectra, but are followed well in the fixed-frequency spectra that have a better resolution.

At temperatures well below T_N, a line resembling a paramagnetic (or ferromagnetic) resonance with $g=2$ appears. In the IR data it is seen as a weak absorption band proportional to the field, as shown, e.g., at 15 K in Fig. 10. The same line is observed in the fixed-frequency spectra at 8.1 T at 225 GHz (see Fig. 12), at 150 GHz, and at 75 GHz. The temperature evolution at 75 GHz is illustrated in Fig. 14. The line intensity at 110 K is comparable to that of the paramagnetic resonance at room temperature. As the temperature approaches T_N from below, the line broadens. It disappears at T_N and reappears as a paramagnetic resonance at higher temperatures.

A small amount of paramagnetic impurities isolated from the antiferromagnetic $LaMnO_3$ matrix cannot cause the strong line that disappears at T_N, nor can the line be described in terms of the ferromagnetic branch of a canted antiferromagnet. The small ferromagnetic moment of the canted AF structure of hole doped $LaSrMnO_3$, e.g., changes drastically the resonance mode diagram but there are no modes which are linear in field nor do they extrapolate to zero frequency at zero field.[13]

An anomalous magnetic resonance is observed in the paramagnetic phase above T_N also. As shown in Figs. 15 and 16, in addition to the $g=2$ resonance there is another line in the fixed-frequency spectra with a resonance field that follows an interesting temperature dependence. A summary of data is plotted in Fig. 13.

Below 170 K, the anomalous line is resolved at low magnetic fields for both 225 and 150 GHz. The resonance field rapidly decreases as T_N is approached from above. We interpret the 150-GHz data between 170 and 250 K as a splitting of two interacting modes. The anomalous mode at low temperatures crosses the paramagnetic $g=2$ mode at about 210 K and at higher temperatures reappears at higher fields. Near the crossing point the $g=2$ ''normal'' paramagnetic-resonance frequency is clearly affected, as seen in Fig. 15, in the 18 K–240 K regime.

The agreement of these observations with the FT-IR absorption measurements (Fig. 17) is less satisfactory than that at low temperatures (Fig. 11). The line splitting seen at fixed frequencies is not observed in the IR study, probably due to inadequate signal-to-noise ratio. Note that the anomalous line is weaker at 225 GHz (Fig. 16) and may be lost in noise in the IR spectra. The anomalous line is strong at 150 GHz, but this is very close to the lower end of the frequency range in IR studies. In fact, for most of the frequency range of

the IR studies the anomalous line is very weak or nonexistent.

In homogeneous materials the antiferromagnetic phase has two modes, and in the paramagnetic phase only one mode is possible. The anomalous resonance, however, is present in both the AF and paramagnetic phases, and therefore, it must arise from inhomogeneities within the sample. Such inhomogeneities may arise from regions with higher than the average La vacancy or surplus oxygen concentration. The inhomogeneous regions must be intimately coupled to the antiferromagnetic or paramagnetic spins, since the anomalous resonances exhibit major changes at the Néel temperature. Small ferromagnetic regions embedded in the antiferromagnetic crystal may be the origin of the anomalous line below T_N. The ferromagnetic regions must be large enough to exhibit a ferromagnetic resonance at $g=2$, but small enough to be strongly affected at the Néel temperature. We have no simple picture for the anomalous line in the paramagnetic region. Phase separation or clustering in these compounds has been suggested by several authors[34,35] and discussed in a recent review by Dagotto *et al.*[2] Further studies are required to see whether the anomalous resonance mode is related to the clustering of a residual small concentration of holes, or is a sign of some large scale inhomogeneity in the compound.

VIII. SUMMARY

Observations of antiferromagnetic resonance in $LaMnO_3$ have been made using magneto-optical far-infrared spectroscopy and traditional ESR methods. In the magneto-optical far-infrared spectroscopy setup, the stoichiometric $LaMnO_3$ sample was oriented with the external magnetic field along the easy axis of magnetization (Faraday geometry). The direction of the far-infrared or microwave unpolarized radiation field was perpendicular to the easy axis. The magnetic-field dependence of the AFMR frequencies at low temperatures (15 K) was found to follow the predictions of the mean-field theory of Kittel and Keffer. The value of the zero-field resonance frequency agrees well with the values found by others.[9,13,18] The temperature dependence of the zero-field AFMR frequency was found to follow the dependence of the magnetic superlattice Bragg scattering intensity measured in the neutron-scattering experiments by Moussa.[9] At temperatures close to T_N, the field dependence of the AFMR did not follow the mean-field theory.

Static susceptibility measurements on our sample indicate the presence of a low-temperature ferromagnetic component. We interpret this result in terms of a canted antiferromagnetic structure. The corresponding symmetry-breaking effect on the spin resonance in the Faraday geometry is too small to see.

In the paramagnetic phase the resonance was close to $g=2$. The splitting induced by the anisotropy field, expected to be in the few tesla range, has not been observed. The absence of the splitting is due to motional narrowing caused by spin exchange and residual mobile electrons.

At low frequencies anomalous, strongly temperature-dependent resonance lines were found. This feature is most likely caused by phase-separated domain(s) in the sample, although no satisfactory model can be offered at this time. In any case, the spins involved in the anomalous resonance are strongly interacting with the ''regular'' paramagnetic (or antiferromagnetic) spins. Further studies are required to see whether the anomalous resonance mode is related to the clustering of residual holes in the sample.

ACKNOWLEDGMENTS

We acknowledge the support from the National Science Foundation (Grants Nos. DMR 0132282 and DMR 9803025), from DARPA/UCLA Grant No. 1000GCG008, from Hungarian state grants (Grants Nos. OTKA TS040878 and T043255), and from the European Infrastructure Network, SENTINEL. The collaboration between Stony Brook University and the Budapest University of Technology was supported by NATO travel grants. The work at the Nation Synchrotron Light Source was supported by the U.S. Department of Energy, under Contract No. DE-AC02-98CH10886.

[1] J.M.D. Coey, M. Viret, and S. von Molnar, Adv. Phys. **48**, 167 (1999).
[2] E. Dagotto, T. Hotta, and A. Moreo, Phys. Rep. **344**, 1 (2001).
[3] G.H. Jonker and J.H. van Santen, Physica (Amsterdam) **16**, 337 (1950).
[4] J. van Santen and G. Jonker, Physica (Amsterdam) **16**, 599 (1950).
[5] E.O. Wollan and W.C. Koehler, Phys. Rev. **100**, 545 (1955).
[6] J.B. Goodenough, Phys. Rev. **100**, 564 (1955).
[7] J.B. Goodenough, in *Progress in Physical Chemistry*, edited by H. Reiss (Pergamon, New York, 1971), Vol. 5, pp. 145–399.
[8] B. Dabrowski *et al.*, Phys. Rev. B **60**, 7006 (1999).
[9] F. Moussa, M. Hennion, J. Rodriguez-Carvajal, H. Moudden, L. Pinsard, and A. Revcolevschi, Phys. Rev. B **54**, 15 149 (1996).
[10] J. Rodríguez-Carvajal, M. Hennion, F. Moussa, A.H. Moudden, L. Pinsard, and A. Revcolevschi, Phys. Rev. B **57**, R3189 (1998).
[11] M.C. Guidi, G. Allodi, R.D. Renzi, G. Guidi, M. Hennion, L. Pinsard, and A. Amato, Phys. Rev. B **64**, 064414 (2001).
[12] R.H. Heffner, J.E. Sonier, D.E. MacLaughlin, G.J. Nieuwenhuys, G.M. Luke, Y.J. Uemura, W. Ratcliff, S.W. Cheong, and G. Balakrishnan, Phys. Rev. B **63**, 094408 (2001).
[13] A. Pimenov, M. Biberacher, D. Ivannikov, A. Loidl, V.Y. Ivanov, A.A. Mukhin, and A.M. Balbashov, Phys. Rev. B **62**, 5685 (2000).
[14] A. Shengelaya, G. Zhao, H. Keller, and K.A. Muller, Phys. Rev. Lett. **77**, 5296 (1996).
[15] C. Rettori, D. Rao, J. Singley, D. Kidwell, S.B. Oseroff, M.T. Causa, J.J. Neumeier, K.J. McClellan, S.-W. Cheong, and S. Schultz, Phys. Rev. B **55**, 3083 (1997).

[16] S.B. Oseroff, M. Torikachvili, J. Singley, S. Ali, S.-W. Cheong, and S. Schultz, Phys. Rev. B **53**, 6521 (1996).
[17] M. Causa, G. Alejandro, R. Zysler, F. Prado, A. Caneiro, and M. Tovar, J. Magn. Magn. Mater. **196-197**, 506 (1999).
[18] S. Mitsudo, K. Hirano, H. Nojiri, M. Motokawa, K. Hirota, A. Nishizawa, N. Kaneko, and Y. Endoh, J. Magn. Magn. Mater. **177-181**, 877 (1998).
[19] A.A. Mukhin, V.Y. Ivanov, V.D. Travkin, A. Pimenov, A. Loidl, and A.M. Balbashov, Europhys. Lett. **49**, 514 (2000).
[20] D. Ivannikov, M. Biberacher, H.-A.F. von Nidda, A. Pimenov, A. Loidl, A.A. Mukhin, and A.M. Balbashov, Phys. Rev. B **65**, 214422 (2002).
[21] V. Skumryev, F. Ott, J.M.D. Coey, A. Anane, J.-P. Renard, L. Pinsard-Gaudart, and A. Revcolevschi, Eur. Phys. J. B **11**, 401 (1999).
[22] L. Mihaly, D. Talbayev, and G. L. Carr, National Synchrotron Light Source activity report, 2001.
[23] P.L. Richards, Phys. Rev. **138A**, 1769 (1965).
[24] R.C. Ohlmann and M. Tinkham, Phys. Rev. **123**, 425 (1961).
[25] C. P. Slichter, *Principles of Magnetic Resonance*, 3rd ed. (Springer-Verlag, Berlin, 1996).
[26] V.Y. Ivanov, V.D. Travkin, A.A. Mukhin, S.P. Lebedev, A. Volkov, A. Pimenov, A. Loidl, A.M. Balbashov, and A.V. Mozhaev, J. Appl. Phys. **83**, 7180 (1998).
[27] F. Keffer and C. Kittel, Phys. Rev. **85**, 329 (1952).
[28] S. Foner, in *Magnetism*, edited by G. T. Rado and H. Suhl (Academic press, New York, 1984), Vol. I.
[29] I. Dzyaloshinski, J. Phys. Chem. Solids **4**, 241 (1958).
[30] T. Moriya, in *Magnetism*, edited by G.T. Rado and H. Suhl (Academic press, New York, 1984), Vol. I, p. 85.
[31] G. Cinader, Phys. Rev. **155**, 453 (1967).
[32] P.-G. de Gennes, Phys. Rev. **118**, 145 (1960).
[33] D.L. Huber, G. Alejandro, A. Caneiro, M.T. Causa, F. Prado, M. Tovar, and S.B. Oseroff, Phys. Rev. B **60**, 12 155 (1999).
[34] M. Hennion, F. Moussa, G. Biotteau, J. Rodirguez-Carvajal, L. Pinsard, and A. Revcolevschi, Phys. Rev. B **61**, 9513 (2000).
[35] S. deBrion, F. Ciorcas, G. Chouteau, P. Lejay, P. Radaelli, and C. Chaillout, Phys. Rev. B **59**, 1304 (1999).